Fluid-Asperity Interaction Induced Random Vibration of Hydrodynamic Journal Bearings towards Early Fault Diagnosis of Abrasive Wear

H. Zhang[*1,3], J. Ma[1,3], X. Li[2], S. Xiao[1], F. Gu[3], A. Ball[3]
[1]*School of Mechanical Engineering, Hebei University of Technology, Tianjin, China, 300130*
[2]*China North Engine Research Institute, Tianjin, China, 300400*
[3]*Centre for Efficiency and Performance Engineering, University of Huddersfield, Huddersfield, United Kingdom, HD1 3DH*

Abstract

One of difficulties to detect abrasive wear in journal bearings through vibration analysis is the lack of obvious fault characteristics in an early stage. To carry out an in-depth investigation on the relationship between wear occurred inside and vibration signals acquired outside is meaningful from the diagnostic point of view. In this paper, a tribo-dynamic model is developed for the fluid-asperity interaction in journal bearings. The microscopic pressure fluctuation induced random excitation is derived. The effects of surface roughness and operating condition on the random excitation are investigated. It is found that wear induced narrowband spatial components of journal surface can excite random vibration of bearing. The speed dependent vibrational behaviour is found to be an effective indicator of surface defects.

Keywords: Journal bearing; fault diagnosis; fluid-asperity interaction; random vibration

1. Introduction

Journal bearings have been widely used in a variety of rotating machineries such as steam turbine, centrifugal compressor, engine crankshaft, etc. After long period of operation, they are susceptible to various types of faults including abrasive wear, sintering, corrosion, erosion, etc. Among those faults, abrasive wear is one of the most typical types that significantly shorten their service lives. To fulfil an efficient condition monitoring for journal bearings and detect the abrasive wear as early as possible are of great significance for normal operation of the whole rotor-bearing system. The parameters available to be monitored generally include vibration signal, lubricant oil temperature, oil debris, background noise, acoustic emission signal, etc [1]. Lubricant oil temperature is often not sensitive to the wear fault until reaching a serious stage. Online oil debris examination usually needs special instruments to be installed on the system [2]. Both noise and acoustic emission signal are susceptible to the background noise. Comparatively, vibration analysis is the most common way with the advantages of low cost, non-invasive and real-time. However, the significant difficulty to detect the wear fault in journal bearings via vibration analysis is the lack of obvious fault characteristics like periodical impulse signals in faulty rolling element bearings especially in an early stage. In addition, the complex transfer path from the excitations inside to the sensors outside would inevitably bring in interference to the useful information. Therefore, to carry out an in-depth investigation on the wear fault induced vibrational behaviours of journal bearings is very meaningful from the diagnostic point of view.

The first quantitative model to evaluate the wear in journal bearings was developed by Dufrane [3] according to the experimental observation from steam turbines which had been operated for a long period. In this model, the shape change of bearing surface was described as an arc at a radius larger than the journal. Based on this model, Hashimoto et al [4] investigated the effects of wear on pressure distribution and static equilibrium position. Recently, Fillon et al [5] carried out a numerical study on tribology and thermal performances of journal bearings subjected to different degree of wear fault. An interesting conclusion was drawn that the wear fault might improve the thermohydrodynamic lubrication performances for both highly loaded bearings and high speed operating bearings. Khonsari et al [6,7] conducted the elastohydrodynamic lubrication (EHL) analysis to predict the wear coefficient under sliding condition. Sander et al [8,9] proposed a lubrication model based on Archard wear law to study the tribology behaviour of a worn journal bearing. Xiang et al [10] developed a transient mixed lubrication and wear coupling numerical model for journal bearings in order to simulate its wear evolution and predict the tribology performance. As can be seen from the published literatures so far, researches regarding the wear concentrated on the macroscopic shape change on the ‘softer’ bearing surface and its influence on either tribology or dynamic performances of journal bearings. As a matter of fact, abrasive wear usually undergoes a dynamic evolution process before the obvious shape change being formed. Hard particles moving in the lubricating friction pair may damage the “smooth” mating surfaces via the mechanism of two-body or three-body abrasive wear [11]. Thus, the surface topography would firstly be affected with the generation of numerous troughs and summits on both surfaces. After a period of evolution, the cumulated macroscopic shape change will be formed obviously on the softer bearing surface. Accordingly, more attentions deserve to be paid on the effects of surface topography changes from the early diagnostic point of view.

The investigation on the effects of surface topography on tribo-dynamic behaviours of journal bearings belongs to a typical multi-scale problem. The approaches to deal with this issue can

roughly be classified into two categories, i.e. stochastic method and deterministic method [12]. In stochastic method, the analysis in local scale and global scale are decoupled. The influences of local changes in film thickness on pressure distribution are statistically averaged and represented by several factors. Substituting these factors into the global scale governing equations, the final solutions can be derived. P&C flow factor method and homogenisation method are two typical stochastic methods. Dobrica and Fillon [13] numerically studied tribology performances of the partial journal bearing being operated within the mixed EHL regime using P&C flow factor method. The comparison with the solution of deterministic method in terms of pressure distribution, minimum film thickness and friction torque demonstrate the satisfactory prediction accuracy of the P&C flow factor method. To further improve P&C flow factor method, Chan et al [14] proposed a parallel numerical iteration algorithm to treat the EHL problem of journal bearings. The solution speed of the modified Reynolds equation and asperities elastic deformation equation was greatly accelerated. Sahlin et al [15,16] studied the effects of surface texture on the 3D mixed lubrication problem using P&C flow factor method and homogenisation method respectively. The significant difference was observed when the surface texture was dominated by the cross mode. In order to reduce the error of homogenisation method generated during the scale transformation, Checo et al [17] considered the change of lubricant density and pressure in local scale when treating the EHL lubrication problem.

Despite the advantages in simplification, the stochastic method cannot well describe the instantaneous film thickness fluctuation as well as the local pressure drop, thus it is unsuitable to treat such tribo-dynamic coupled analysis. To address this issue, the deterministic method should be adopted. Wang et al [18] analysed the EHL performances of five kinds of engineering surfaces, including honed, turned, isotropically finished, ground, and dimpled surfaces. The measured surface topographies were directly substituted into the lubrication governing equations. The numerical results demonstrated the dependency of lubrication on the surface finish orientation. For tribo-dynamic performances of piston ring in the internal combustion engines, Meng et al [19,20] developed a multi-scale thermoelastohydrodynamic lubrication (TEHL) model, based on which the effects of surface texture on ring, liner, skirt on lubrication characteristics were studied using deterministic method. It was found that the appropriate surface texture on ring and skirt could efficiently reduce the friction loss especially at high speed. Wang et al [21] developed a model for the journal bearing in which the surface waviness was simplified to be a sinusoidal shape. Based on the numerical analysis, the effects on the static and dynamic characteristics of the journal bearing were analysed. In order to shorten the numerical computation time, a robust algorithm for analysing the surface texture effects in journal bearings was developed by Quiñonez et al [22], who adopted the perturbation technique coupled with linear superposition using Fourier transforms. As can be seen from the published literatures, the application of deterministic approach is generally limited to the analysis of those point-contact, line-contact EHL or mixed lubrication, such as rolling element bearing, gears, due to the demand of large discretisation effort. Journal bearings operating within hydrodynamic lubrication (HL) regime have a surface-surface contact friction pair, which contact area is rather larger compared to the asperities. Therefore, the treatment to the tribo-dynamic analysis for hydrodynamic journal bearings is still a challenging task.

This paper aims to clarify the excitation mechanism of fluid-asperity interaction (FAI) occurred in journal bearings working within HL regime, and to establish the relationship between the surface

topography and the correlated random vibration. The structure of this paper is organised as follows: following this introduction, the mathematical model for FAI in journal bearings working within HL regime is developed. The microscopic pressure fluctuation (MPF) induced random excitation is studied by the aid of the generated Gaussian rough surface, according to the theory of random vibration. Based on the theoretical analysis, numerical simulation is then carried out to evaluate the effects of surface roughness and operating conditions on the random excitations. Finally, relevant experiments are conducted to verify the observation from the simulation results. This research will pave a theoretical foundation for the condition monitoring on journal bearings and the fault diagnosis of abrasive wear in an early stage.

2. Theory

2.1. Fluid-asperity interaction

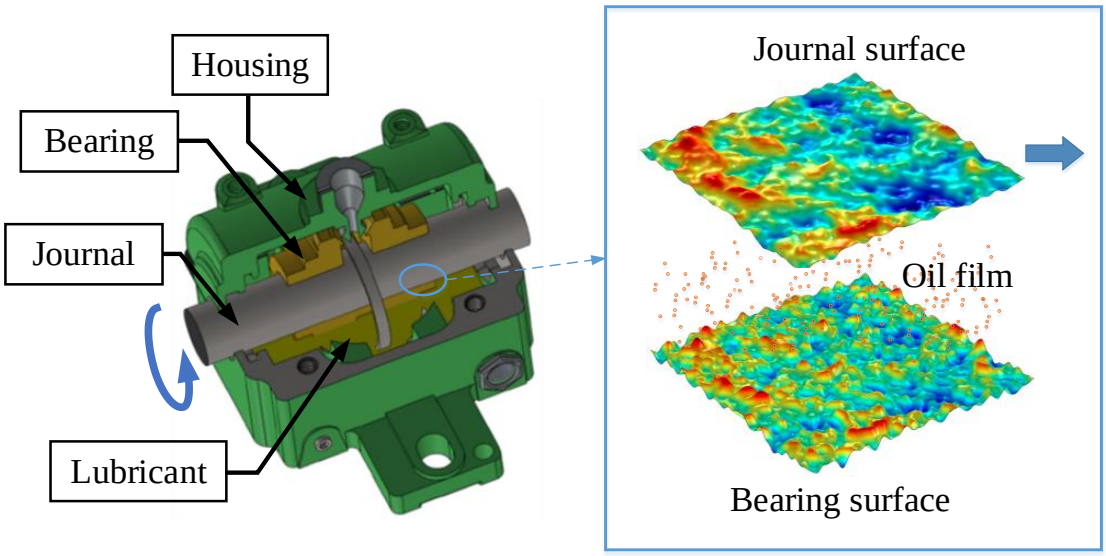

Figure 1. Schematic of fluid-asperity interaction in journal bearings working within HL regime

As shown in Fig. 1, the main components of journal bearings generally include journal, bearing (usually with housing outside) and fluid film in the clearance. Whilst in operation, viscous lubricant oil flows in the bearing clearance driven by the rotational journal generating the hydrodynamic force to support radial load. The rotor-bearing system is likely subject to the external forces due to residual unbalance, misalignment, etc. Those forces could excite the journal bearing to vibrate at frequencies of the rotational speed and its sub-harmonics, harmonics and super-harmonics. Besides, the system may also subject to those broadband random excitations possibly induced by FAI, cavitation, turbulent flow, background noise, etc. Under such broadband excitations, the resonant vibration of the rotor-bearing system may be excited around its natural frequencies, which usually distribute within a rather wide frequency band. Herein, more attention deserves to be paid on the FAI induced random vibration because the valuable information regarding the surface topography might be hidden in it. By the aid of amplification of the resonant vibration, the wear fault is possible to be detected from such random vibration.

In practice, it is impossible to machine a perfectly smooth surface. There must be a huge number of asperities randomly distributed on it from the microscopic point of view. Even if the shaft

steadily rotates around its equilibrium position, the time-varying fluid film thickness due to rotating rough journal surface could give rise to the phenomenon of MPF acted on journal and bearing simultaneously. The whole rotor-bearing system would thereby be excited to perform the broadband random vibration. The FAI here can be interpreted as a simplified case of Fluid-Structure Interaction (FSI) in the micro scale with such complicated phenomenon as micro cavitation, micro vortex, elastic deformation of asperities being ignored. In what follows, a study on the FAI induced MPF in the fluid film will be carried out and the effects of surface topography and operating condition on the random excitation will be clarified.

2.2. Microscopic pressure fluctuation induced random excitations

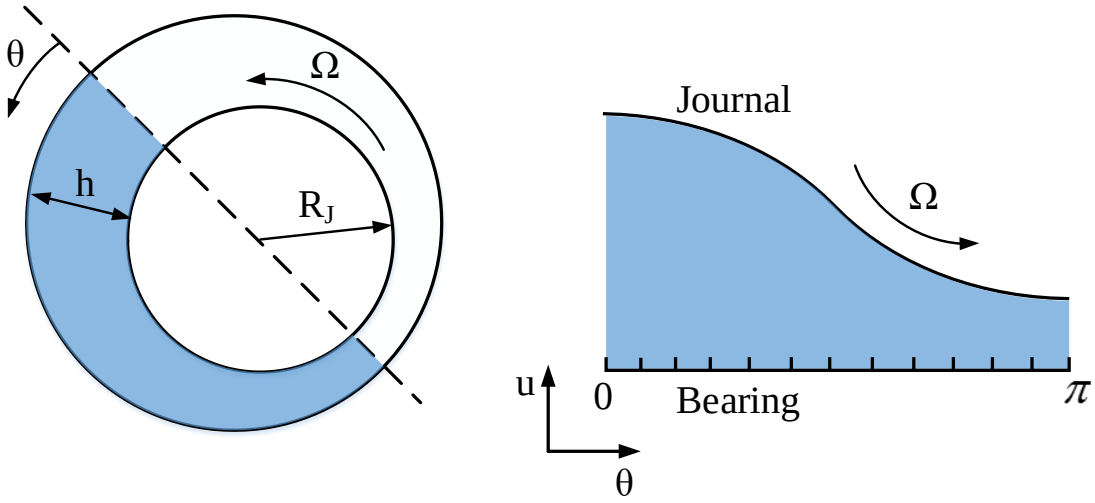

Figure 2. Tribo-dynamic coupled model of journal bearings

Due to the properties of randomness in both time and space domains, it is impossible to derive the exactly analytical expression regarding the MPF induced random excitations. Moreover, it is also unrealistic to discretise the whole fluid film land to the roughness scale, which would result in an unaffordable number of grids. Thus, the excitations must be treated from a statistical point of view. The MPF in hydrodynamic journal bearings can be treated to be the response of rotating journal surface as a displacement excitation through the fluid film as a transfer path, which can be evaluated by its equivalent frequency response function (FRF). According to the theory of random vibration, their relationship can be expressed as

$$S_P(\omega) = |H(\omega)|^2 S_J(\omega) \tag{1}$$

where $S_J(\omega)$ and $S_P(\omega)$ respectively denotes the auto power spectral density (APSD) of the displacement excitation and the resulted MPF, $H(\omega)$ denote FRF of the fluid film.

To evaluate the displacement excitation and FRF involved in eq. (1), a simplified tribo-dynamic coupled model is developed, which is shown in Fig. 2. In this model, MPF is assumed to be limited within the convergent oil wedge approximately from $\theta = 0$ to $\theta = \pi$. The journal is restricted to be rotating around its own axis without any vibration, and the bearing is assumed as a rigid body with only one degree of freedom. The motion of bearing is determined by the distributed loads due to MPF. For simplicity, infinitely long bearing theory is adopted to carry out the qualitative analysis.

Given this tribo-dynamic coupling model, eq. (1) is rewritten into eq. (2)

$$S_P(\omega) = R_J^2 \int_0^{\pi} \int_0^{\pi} H_i(j\omega) H_j(-j\omega) S_J(\theta_j, \theta_i, \omega) d\theta_i d\theta_j \tag{2}$$

where $S_J(\theta_j, \theta_i, \omega)$ denotes the cross power spectral density (CPSD) of displacement excitations at the positions of θ_j and θ_i, $H_i(j\omega)$ and $H_j(-j\omega)$ denote the corresponding FRFs of fluid film, R_J is the radius of journal. To facilitate numerical evaluation, the continuous fluid film is discretised into n segments within which an equivalent concentrated excitation act. Thereby, the distributed excitation is approximately replaced by n concentrated excitations. The corresponding APSD of MPF $S_P(\omega)$ can then be expressed in eq. (3).

$$S_P(\omega) \approx \left(R_J \Delta\theta\right)^2 \sum_{i,j=1}^{n} H_i(j\omega) H_j(-j\omega) S_J(\theta_j, \theta_i, \omega) \tag{3}$$

Coming from the same rotating journal surface, the displacement excitation in the fluid film is directly related to the surface topography of journal in circumferential direction. Moreover, the displacement excitations possess the characteristics of time-lag. Assumed the shaft steadily rotating at a constant angular speed of Ω, the displacement excitations $\delta(\theta_j, t)$ and $\delta(\theta_i, t)$ at the positions of θ_j and θ_i satisfy the following relationship:

$$\delta(\theta_j, t) = \delta(\theta_i, t + \tau_0) \tag{4}$$

where the time-lag $\tau_0 = (\theta_j - \theta_i)/\Omega$.

Due to the property of time-lag, the CPSD $S_J(\theta_j, \theta_i, \omega)$ of displacement excitations can be expressed in eq. (5).

$$S_J(\theta_j, \theta_i, \omega) = e^{-j\omega\tau_0} S_J(\theta_i, \omega) \tag{5}$$

where $S_J(\theta_i, \omega)$ represents the APSD of displacement excitation at the position of θ_i.

In essence, the time-lag excitations can be viewed as a special case of excitations that are directly correlated. Both the autocorrelation function and APSD of displacement excitations are independent with the position. Hence, eq. (5) can be rewritten into eq. (6)

$$S_J(\theta_j, \theta_i, \omega) = e^{-j\omega\tau_0} S_J(\omega) \tag{6}$$

Substituting eq. (6) into eq. (3), yields the APSD of MPF expressed in eq. (7).

$$S_P(\omega) \approx \left| \sum_{i=1}^{n} H_i(j\omega) e^{j\omega(i-1)\tau_0} \right|^2 S_J(\omega) \tag{7}$$

The APSD of displacement excitation $S_J(\omega)$ is determined by the spatial spectrum of journal surface and its linear velocity. Their relationship is given as follows

$$S_J(\omega) = (\Omega R_J)^{-1} S_J^{(s)}(\gamma \Omega R_J) \tag{8}$$

where $S_J^{(s)}(\gamma \Omega R_J)$ represents the spatial spectrum of journal surface, γ is its wavenumber.

Given the above derivation, it is clear that for the journal with known surface topography, the MPF can be evaluated if only the equivalent FRF of fluid film can be obtained.

2.3. Equivalent FRF of fluid film

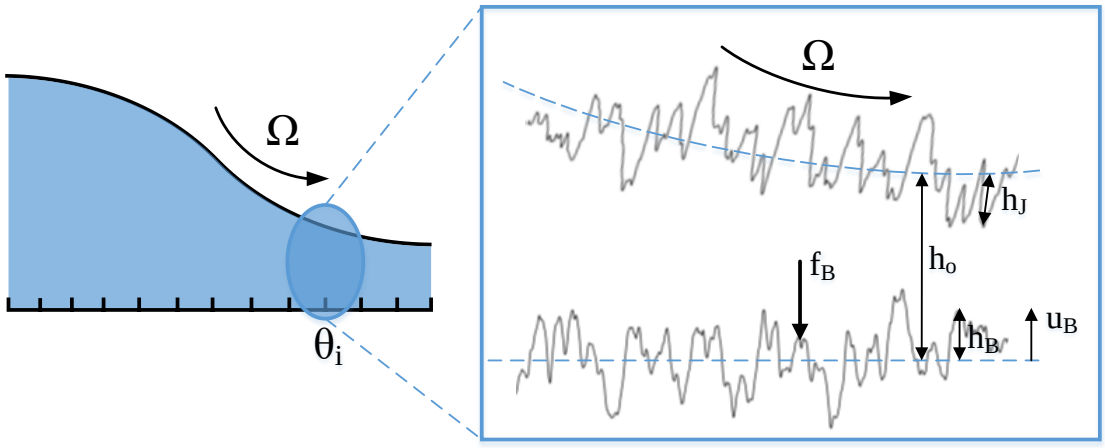

Figure 3. The lubricating friction pair of a journal bearing with rough surfaces

To evaluate FRF of the fluid film at the position θ_i, the tribo-dynamic coupled analysis is carried out within a small area around θ_i, where refined grids can be discretised to the roughness scale. Considering rough surfaces of both journal and bearing, the fluid film thickness h can be expressed as follows:

$$h = h_o + h_J + h_B + u_B \tag{9}$$

where $h_o=C(1+\varepsilon\cos\theta)$ denotes the nominal film thickness, C is the bearing clearance, ε is the eccentricity ratio, h_J and h_B respectively denote the surface heights of journal and bearing, u_B denotes the bearing's motion, f_B denotes the equivalent concentrated force exerted on the bearing within such area. Pressure distribution p within such area is governed by the Reynolds equation expressed in eq. (10)

$$\frac{\partial}{\partial\theta}\left(h^3\frac{\partial p}{\partial\theta}\right) = 6\mu R_J^2\Omega\frac{\partial h}{\partial\theta} + 12\mu R_J^2\frac{\partial h}{\partial t} \tag{10}$$

where μ is the dynamic viscosity of lubricant oil.

Converting eq. (10) to the dimensionless form, yields eq. (11)

$$\frac{\partial}{\partial\theta}\left(H^3\frac{\partial P}{\partial\theta}\right) = \frac{\partial H}{\partial\theta} + 2\frac{\partial H}{\partial\tau} \tag{11}$$

with the dimensionless parameters listed as follows:

$$H = H_o + H_J + H_B + U_B,\ \ H_o = h_o/C,\ H_J = h_J/C,\ \ H_B = h_B/C,\ \ U_B = u_B/C,\ \ \tau = \Omega t,$$

$$P = p/\tilde{P},\ \ \tilde{P} = 6\mu\Omega\left(R_J/C\right)^2.$$

Expanding the terms on right hand side of eq. (11), generates eq. (12)

$$\frac{\partial H}{\partial\theta} + 2\frac{\partial H}{\partial\tau} = \frac{\partial H_o}{\partial\theta} + \frac{\partial H_J}{\partial\theta} + \frac{\partial H_B}{\partial\theta} + 2\frac{\partial H_o}{\partial\tau} + 2\frac{\partial H_J}{\partial\tau} + 2\frac{\partial U_B}{\partial\tau} \tag{12}$$

Since the dimensionless time dependent variable H_J comes from the rotation of journal surface, it can be written in eq. (13) [23]:

$$H_J = H_J\left(\theta - \tau\right) \tag{13}$$

Hence,

$$\frac{\partial H_J}{\partial \tau} = -\frac{\partial H_J}{\partial \theta} \tag{14}$$

Substituting eq. (14) into eq. (12) and (11), yields eq. (15)

$$\frac{\partial}{\partial \theta}\left(H^3 \frac{\partial P}{\partial \theta}\right) = -\varepsilon \sin\theta - \frac{\partial H_J}{\partial \theta} + \frac{\partial H_B}{\partial \theta} + 2\frac{\partial U_B}{\partial \tau} \tag{15}$$

An appropriate boundary condition must be predefined to numerically solve eq. (15). Since the surface height of journal is generally at the order of micron, the micro cavitation is unlikely to form within the convergent wedge due to the extreme high ambient pressure. It is therefore reasonable to ignore the cavitation effect and assume the continuous fluid flow. The MPF can be obtained through the numerical solution of eq. (15) with a periodic boundary condition.

The equivalent force acted on the bearing f_B can be obtained by the time-varying pressure fluctuation $P(\theta_i, t)$ at the position θ_i multiplied by the area $R_J \Delta\theta$.

$$f_B = \left(P\left(\theta_i, t\right) R_J \Delta\theta\right)\tilde{P} \tag{16}$$

The bearing's motion is governed by eq. (17).

$$m_B \ddot{u}_B = f_B \tag{17}$$

Solving eqs. (15), (16) and (17) simultaneously, the square of the FRF of fluid film at the position of θ_i can be estimated by eq. (18).

$$\left|H_i\left(j\omega\right)\right|^2 = S_P\left(\theta_i, \omega\right) / S_J\left(\omega\right) \tag{18}$$

Following the FRFs of all segments being obtained, the equivalent FRF of the whole fluid film can be calculated by eq. (7).

2.4. Generation of Gaussian rough surface

To carry out the numerical study on tribo-dynamics behaviours of journal bearings, it is necessary to predefine the rough surfaces given some representative statistical parameters. A Gaussian rough surface can be well described by two statistical parameters, standard deviation and correlation length, which represent the information of surface height and spatial frequency, respectively. For a non-Gaussian rough surface, two additional statistical parameters that are skewness and kurtosis need to be added to describe the asymmetric spread and peakedness of height distribution. Since such complicated micro-scale fluid dynamics as micro cavitation, micro vortex, elastic deformation of asperities are ignored here and only the moving rough boundary induced microscopic pressure fluctuation is evaluated, there would be no essential difference between Gaussian rough surface and non-Gaussian rough surface. In this paper therefore, Gaussian rough surfaces are generated. The approach to numerically generate the rough surfaces is based on the Fast Fourier Transform (FFT) along with digital filter proposed by Hu and Tonder [24]. The generation procedure is summarised as follows.

Let a 1D sequence of Gaussian distributed random numbers η with the prescribed standard deviation passes through a digital filter h_f which is designed according to the correlation length,

the output 1D sequence q will be the rough surface to be generated.

$$q(i)=\sum_{v=0}^{n-1}h_f(v)\eta(i+v) \quad i=0,1,...,n-1 \tag{19}$$

In order to design an appropriate digital filter, conducting the Fourier transform to eq. (19), yields

$$\tilde{Q}(\omega)=\tilde{H}_f(\omega)\tilde{\eta}(\omega) \tag{20}$$

where $\tilde{Q}(\omega),\tilde{\eta}(\omega)$ are the Fourier transform of the output and input sequences respectively, $\tilde{H}_f(\omega)$ denotes the transfer function.

The spectral density of output sequence can simply be obtained through FFT of the predefined autocorrelation function, while the spectral density of input sequence is a constant. The transfer function $\tilde{H}_f(\omega)$ can therefore be derived.

$$\tilde{H}_f(\omega)=\sqrt{S_q(\omega)/S_\eta(\omega)} \tag{21}$$

where $S_q(\omega),S_\eta(\omega)$ are the spectral density of output and input sequences, respectively.

3. Simulation Results and Discussions

3.1. Microscopic pressure fluctuation

In this section, numerical simulation is carried out to study the FAI induced random excitations in journal bearings working within the HL regime. The effects of operating condition and surface roughness on the MPF are evaluated. Then, the influences of worn journal surface on the correlated random excitation are analysed.

The radius and clearance of journal bearing are set as 17.5mm and 100μm, respectively. Ignoring thermal effects, a constant dynamic viscosity of lubricant oil is given as 0.012Pas. The oil film land is equally discretised into 40 segments, within which the corresponding FRFs are calculated. In order to reach the roughness scale, the lubricating friction pair of 1mm length rough surfaces is meshed to 4000 grids. Five layers multi-grid numerical scheme is adopted to accelerate the convergence rate. All of equations are programmed and solved using the MATLAB software. Specifically, the Reynolds equation (15) for microscopic pressure fluctuation is solved by finite difference method, and the kinetic equation (17) for bearing's motion is solved by the function ode45.

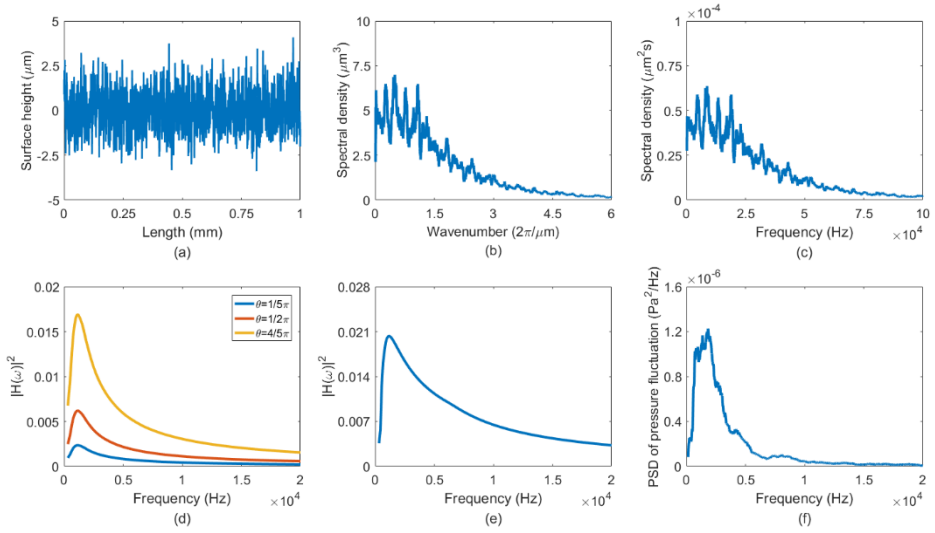

Figure 4. Microscopic pressure fluctuation: (a) Surface topography of journal (b) Spatial spectral density (c) Spectral density of displacement excitation (d) Square of FRFs at different positions (e) Square of equivalent FRF (f) PSD of the resulted MPF

Gaussian rough surfaces are numerically generated and the standard deviations σ are set as 1μm for surface heights of both journal and bearing. The autocorrelation function, which is used to control the power distribution of spatial components, is assumed to be exponential $h_f = \sigma^2 e^{-2.3x/\beta}$ with the correlation length β of 0.8μm and 5.0μm for journal and bearing, respectively. It is noted that correlation lengths are artificially increased here for both journal and bearing to let more spatial components of generated surfaces being distributed within relatively low frequency band, which could reduce the discretisation burden. It would not affect the qualitative analysis of microscopic pressure fluctuation. The rotational speed and eccentricity ratio are given as 600rpm and 0.2. Fig. 4(a)-(c) show the surface topography of journal, its spatial spectral density, and the resulted broadband displacement excitation. The square of FRFs of the fluid film at the positions of 1/5π, 1/2π and 4/5π are shown in Fig. 4(d). It can be seen that the amplitude amplification ratio between MPF and displacement excitation is related to the position in the fluid film. The closer to the position of minimum film thickness, the larger value the amplification ratio. Moreover, the amplification ratios are different for different frequency components. After a maximum amplification ratio at a relatively low frequency, the higher frequency the displacement excitation, the lower the amplification ratio appears. It is demonstrated that surface components with low spatial frequencies could form stronger pressure fluctuation than those with high spatial frequencies. Multiplying the displacement excitation shown in Fig. 4(c) by the square of equivalent FRF shown in Fig. 4(e), yields the PSD of MPF, which is shown in Fig. 4(f). The fluctuation exists within a rather wide frequency range, but unlike white noise, most of the power distributes within the relatively low frequency range. The covered frequency bandwidth depends simultaneously on the spatial spectral density of journal surface and the rotational speed.

3.2. *Effects of operating condition on random excitation*

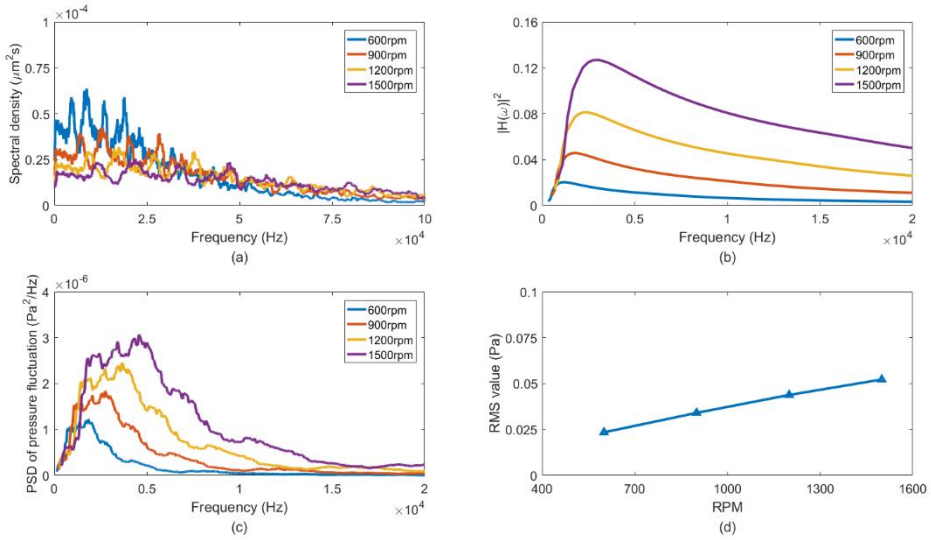

Figure 5. Effects of rotational speed on random excitation: (a) Spectral density of displacement excitation (b) Square of equivalent FRF (c) PSD of the resulted MPF (d) Excitation intensity below angular frequency of 10kHz

Besides the rotational speed, other simulation parameters remain the same as those in section 3.1. For the same journal surface rotating under different speeds, the FAI induced random excitations are illustrated in Fig. 5. As the rotational speed increases, the spectral density of displacement excitation flattens out. The amplitude amplification ratio between MPF and displacement excitation increases within the whole frequency range. The resulted MPF that is shown in Fig. 5(c) demonstrates that the increasing speed would not only increase the amplitude of fluctuation, but also extend the covered frequency bandwidth. As shown in Fig. 5(d), the fluctuation intensity shows an upward trend within the frequency range below angular frequency of 10kHz, which is the frequency response range for most of accelerometers. It should be noted that the assumption of constant eccentricity ratio might introduce some error here, since the change of rotational speed would inevitably lead to the change of eccentricity ratio.

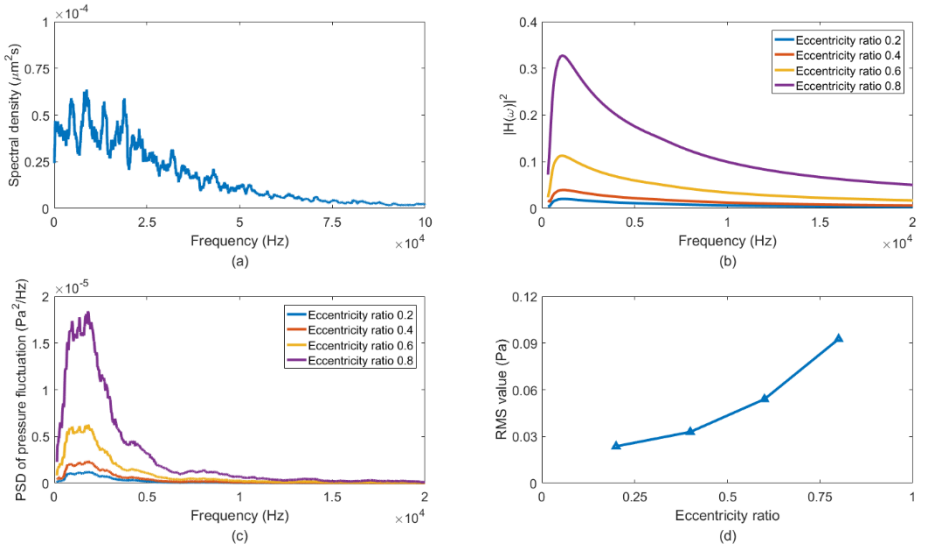

Figure 6. Effects of eccentricity ratio on random excitation: (a) Spectral density of displacement

excitation (b) Square of equivalent FRF (c) PSD of the resulted MPF (d) Excitation intensity below angular frequency of 10kHz

Fig. 6 shows the MPF induced random excitations under different eccentricity ratio, where other simulation parameters remain the same as those in section 3.1. As the eccentricity ratio increases, the minimum fluid film thickness decreases, and thereby the amplitude amplification ratio increases. The stronger intensity of MPF is therefore excited under the same displacement excitation.

3.3. *Effects of surface roughness on random excitation*

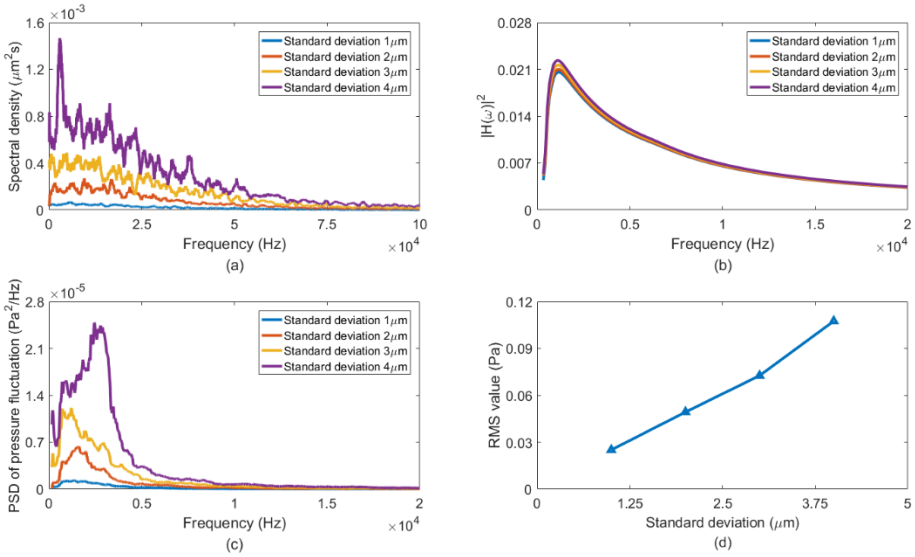

Figure 7. Effects of standard deviation of journal surface on random excitation: (a) Spectral density of displacement excitation (b) Square of equivalent FRF (c) PSD of the resulted MPF (d) Excitation intensity below angular frequency of 10kHz

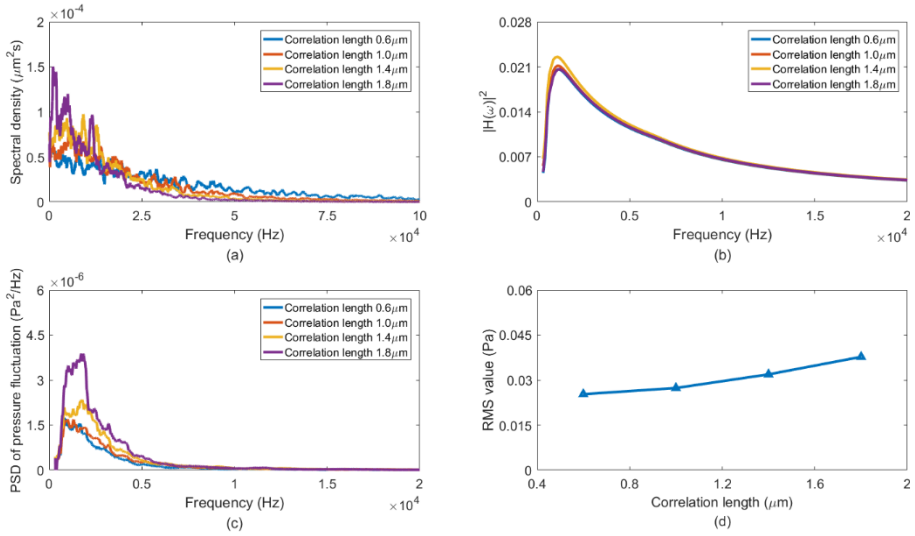

Figure 8. Effects of correlation length of journal surface on random excitation: (a) Spectral density of displacement excitation (b) Square of equivalent FRF (c) PSD of the resulted MPF (d) Excitation intensity below angular frequency of 10kHz

The effects of surface roughness of the journal on random excitation are illustrated in Figs. 7 and 8. Standard deviation and correlation length respectively denote the information of surface height and spatial frequency. It can be seen that as the standard deviation of journal surface increases, the corresponding displacement excitation rises. The intensity of MPF enlarges obviously as surface height of journal increases. The correlation length governs the power distribution of displacement excitation in frequency spectrum. As the correlation length rises, more power distributes within the relatively low frequency range. The equivalent FRF nearly remain the same. The intensity of the resulted MPF increases slightly below angular frequency of 10kHz.

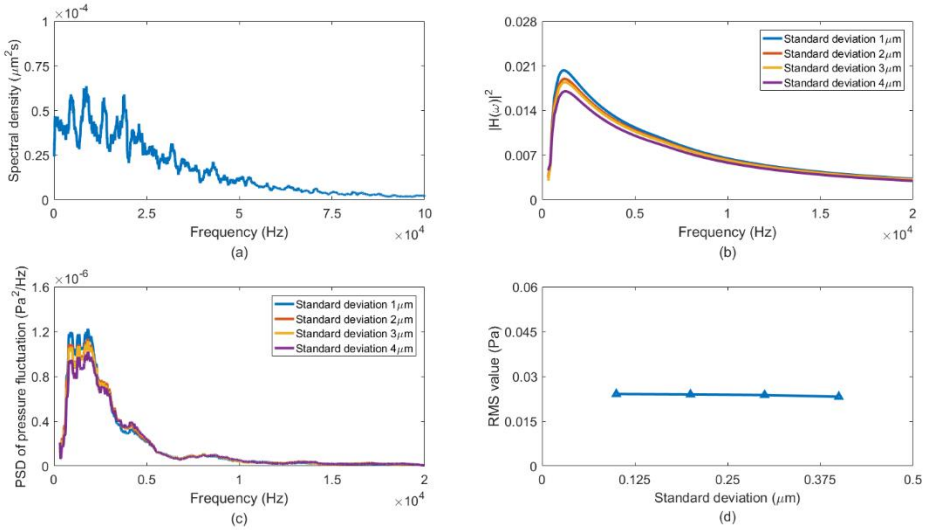

Figure 9. Effects of standard deviation of bearing surface on random excitation: (a) Spectral density of displacement excitation (b) Square of equivalent FRF (c) PSD of the resulted MPF (d) Excitation intensity below angular frequency of 10kHz

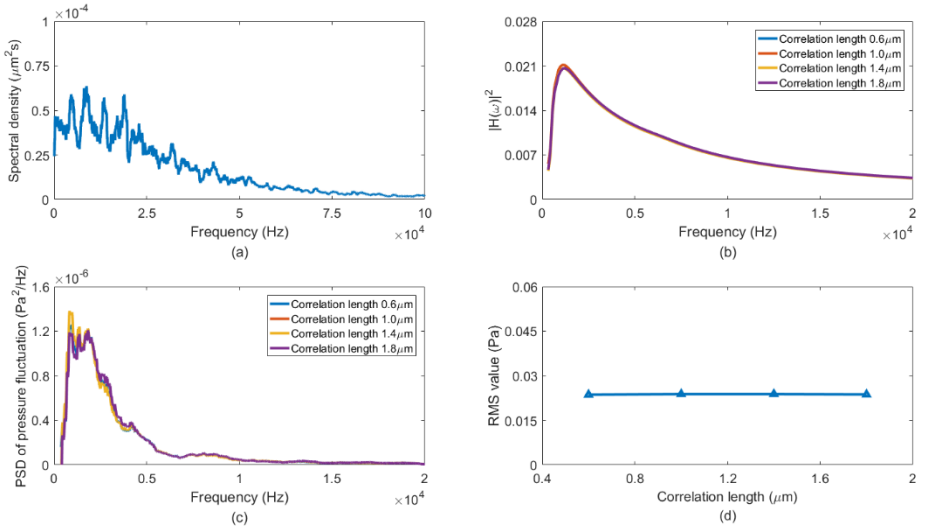

Figure 10. Effects of correlation length of bearing surface on random excitation: (a) Spectral density of displacement excitation (b) Square of equivalent FRF (c) PSD of the resulted MPF (d) Excitation intensity below angular frequency of 10kHz

Figs. 9 and 10 show the effects of surface roughness of the bearing on the random excitation. The bearing surface could only affect the equivalent FRF of fluid film. As the standard deviation of

bearing surface increases, a slight decrease trend of amplitude amplification ratio is observed within the frequency range below 5,000Hz, and thus the resulted MPF slightly decreases within the corresponding frequency range. In addition, the correlation length of bearing surface has little effect on the random excitation.

3.4. *Effects of worn journal on random excitation*

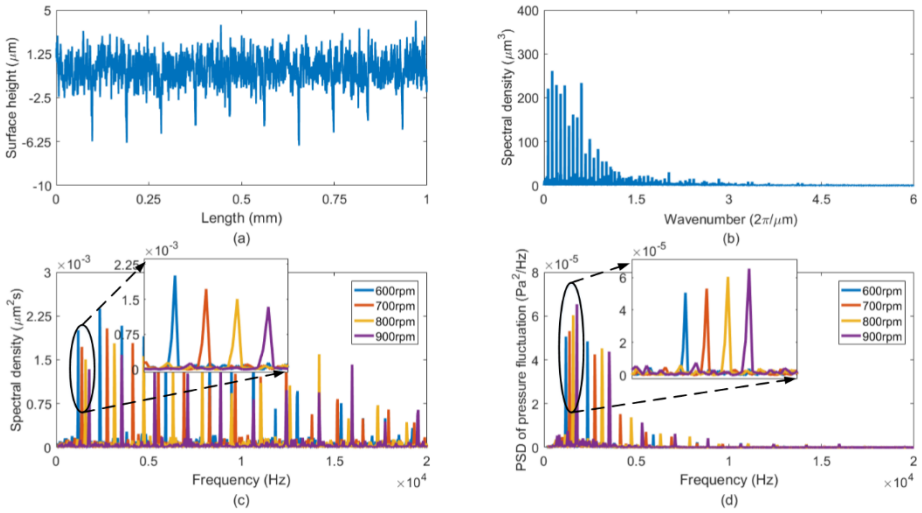

Figure 11. Effects of worn journal on random excitation: (a) Surface topography of a worn journal (b) Spatial spectral density (c) Spectral density of displacement excitation under different rotational speed (d) PSD of the resulted MPF

According to the simulation results regarding the "healthy" rough surfaces with the continuous spatial spectral density, it can be deduced that the MPF induced random excitation depend significantly on the surface roughness of the rotating journal and the operating condition. The journal's surface roughness mainly affects either amplitude or power distribution of the displacement excitation, while the operating condition mainly affects the equivalent FRF of fluid film. For the occurrence of abrasive wear in journal bearings, the hard particles would inevitably damage the rotating journal surface to a certain degree via the mechanism of two-body or three-body abrasion, which might result in a number of microscopic valleys on the originally smooth surface. The surface topography change of the journal would thereby affect the random excitation as well as the vibrational behaviours of the bearing.

As shown in Fig. 11(a), a number of valleys are artificially superposed on the original journal surface. The shapes of valleys are assumed as the isosceles triangles with the width of 10μm and the depth of 5μm. As shown in Fig. 11(b), with the introduction of such valleys, the continuous spatial spectral density of journal changes and a number of narrowband components appear especially within the relatively low frequency range. The amplitudes of such components depend on both width and depth of valleys. Either deeper or wider valleys would give rise to larger amplitudes of such narrowband components. With the journal spins, as shown in Fig. 11(c), narrowband components with obviously large amplitudes also appear in the frequency spectrum of displacement excitations and the resulted MPF. As the rotational speed increases, such narrowband components move to higher frequency band and the corresponding bandwidths become wider. The resonant vibrations of the bearing distributed within the covered frequency band are likely to be

excited with obviously large amplitudes.

4. Experimental Validation

4.1. Test procedure

In this section, the experimental study is carried out to validate the observation from the numerical simulation. As shown in Fig. 12, a self-aligning journal bearing SA35M is adopted here as the tested bearing with the radius and length of 17.5mm and 76.1mm, respectively. Operational modal analysis (OMA) is firstly conducted on the bearing with housing to estimate the distribution of its natural frequencies. Three shafts are manufactured. The journals where fit with the bearings are processed into different surface roughness. Their surface topographies are measured via the Alicona Infinite Focus microscope within a field of 419μm×318μm.

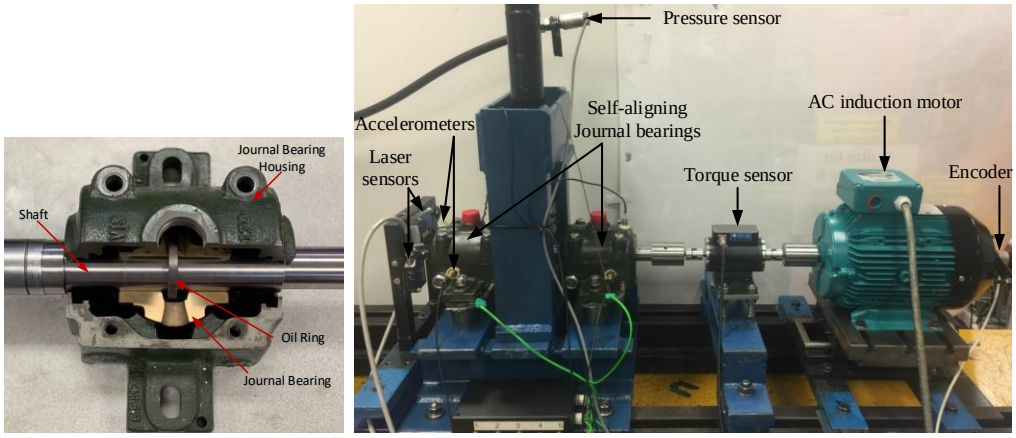

(a) (b)

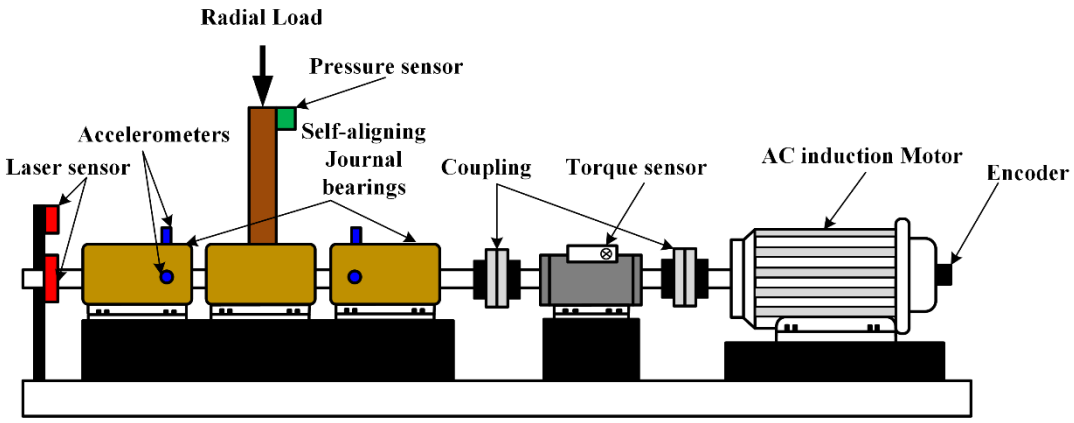

(c)

Figure 12. (a) Tested journal bearing SA35M, (b) Photograph of rotor-bearing test rig, (c) Schematic of rotor-bearing test rig

After the measurement, the shafts are then successively mounted on the rotor-bearing test rig (Fig. 12) supported by a pair of tested bearings. Another journal bearing placed in the midspan of the shaft is used to exert the external load through a hydraulic device. An AC induction motor drives the shaft via a torque sensor. The integrated electronics accelerometers CA-YD-182A, which have a linear frequency response ranging from 1Hz to 10kHz and the sensitivity 2.00 mV/ms^{-2}, are attached outside the housing to acquire its random vibration. A pair of optoNCDT1402 laser

sensors from Micro-Epsilon are used to monitor the shaft trajectory. Following the installation, measurements are then carried out on the random vibration of journal bearings that operate under different surface roughness and operating conditions.

4.2. Operational modal analysis

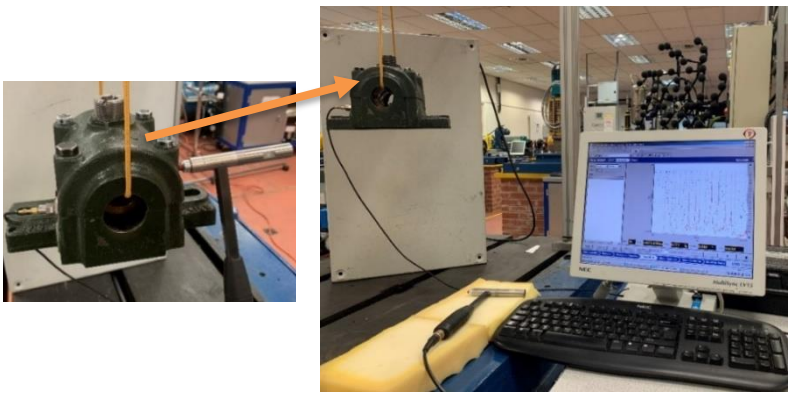

Figure 13. Free modal analysis for the tested bearing

Free modal analysis is firstly carried out on the tested bearing to have an estimation of its modal parameters within the frequency range of interest. As shown in Fig. 13, the tested bearing with housing is suspended through a long elastic rope. Using a hammer to excite it, the broadband responses from 1Hz to approximate 10kHz are acquired via accelerometers. Using LMS test system, the free modal parameters are identified and listed in Table 1.

Table 1 Free modal parameters of the tested journal bearing, SA35M

Mode	Natural frequency (Hz)	Damping ratio (%)
①	1734	1.27%
②	2434	1.32%
③	2875	0.82%
④	3603	0.57%
⑤	5388	0.67%
⑥	6706	0.48%
⑦	6919	0.25%
⑧	7928	0.30%
⑨	8441	0.41%

Whilst in operation, the tested bearing is constrained by both base and fluid film, which would affect the distribution of natural frequencies. Stochastic subspace identification (SSI) approach is adopted to identify its operational modal parameters from the broadband random vibration of journal bearing. For detailed algorithm of this identification method, please refer to the third chapter of Ref. [25]. The identified operational modal parameters of such modes corresponding to the free modal parameters are listed in Table 2.

Table 2 Operational modal parameters of the tested journal bearing, SA35M

Mode	Natural frequency (Hz)	Damping ratio (%)
①	2293	2.03%
②	2866	1.18%
③	3323	0.85%

④	4638	2.37%
⑤	5142	2.39%
⑥	6896	2.05%
⑦	7261	1.20%
⑧	8227	0.13%
⑨	9359	1.67%

4.3. Effects of surface roughness of journal on random vibration

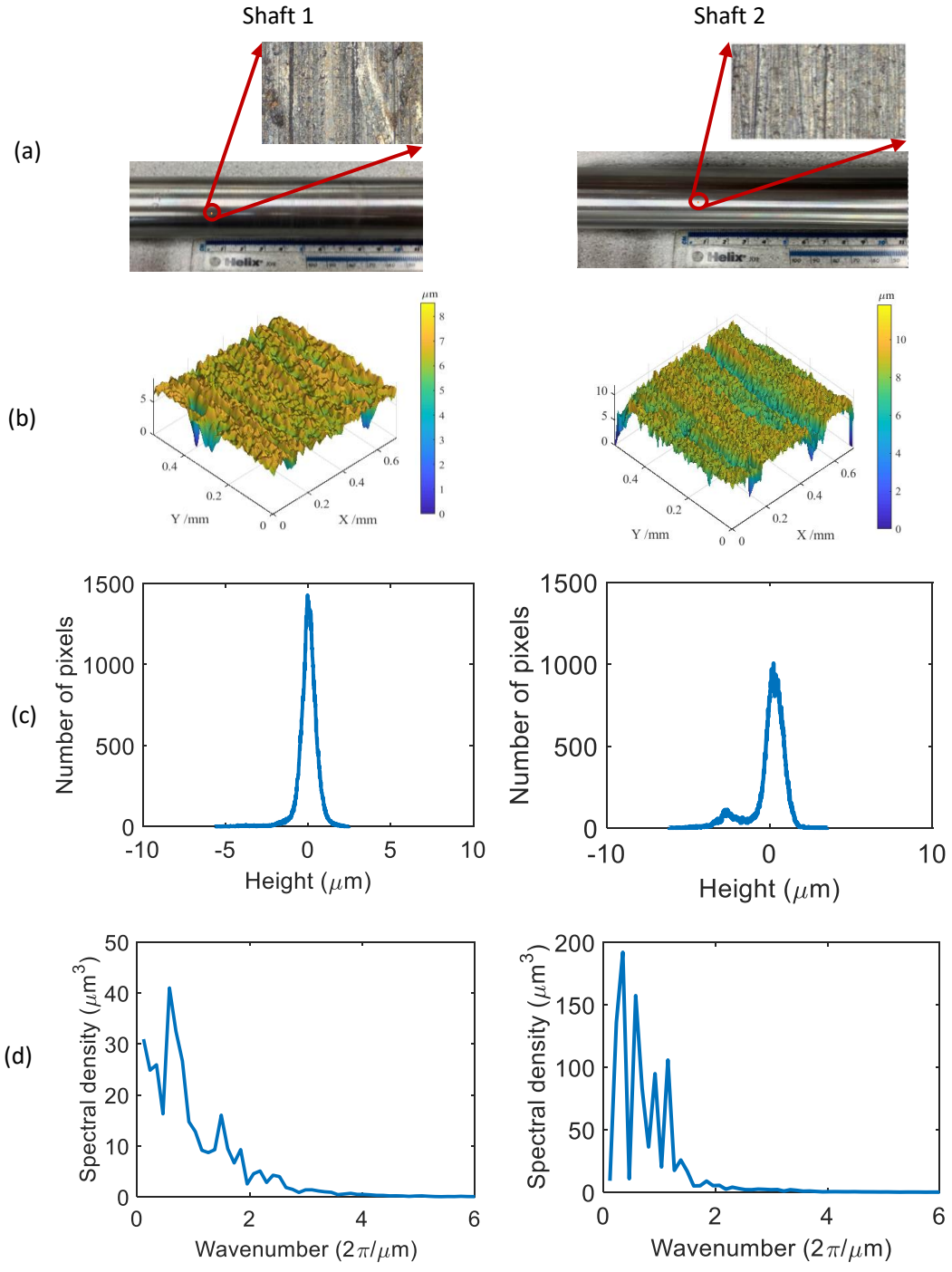

Figure 14. Surface topographies of journals on two shafts with different surface roughness: (a) photomicrograph (b) 3D profile (c) asperities' height distribution (d) spectral density

Surface topographies of journals with different surface roughness are shown in Fig. 14. Ra of the journal on shaft 1 is 0.96μm, and Ra of the journal on shaft 2 is 1.63μm. It can be seen that the distribution of surface height basically exhibit Gaussian distribution characteristics. For the spatial distribution, most of components distribute below the spatial frequency of 2 (2π/μm). The amplitudes of low spatial frequency components on shaft 2 are larger than that on shaft 1.

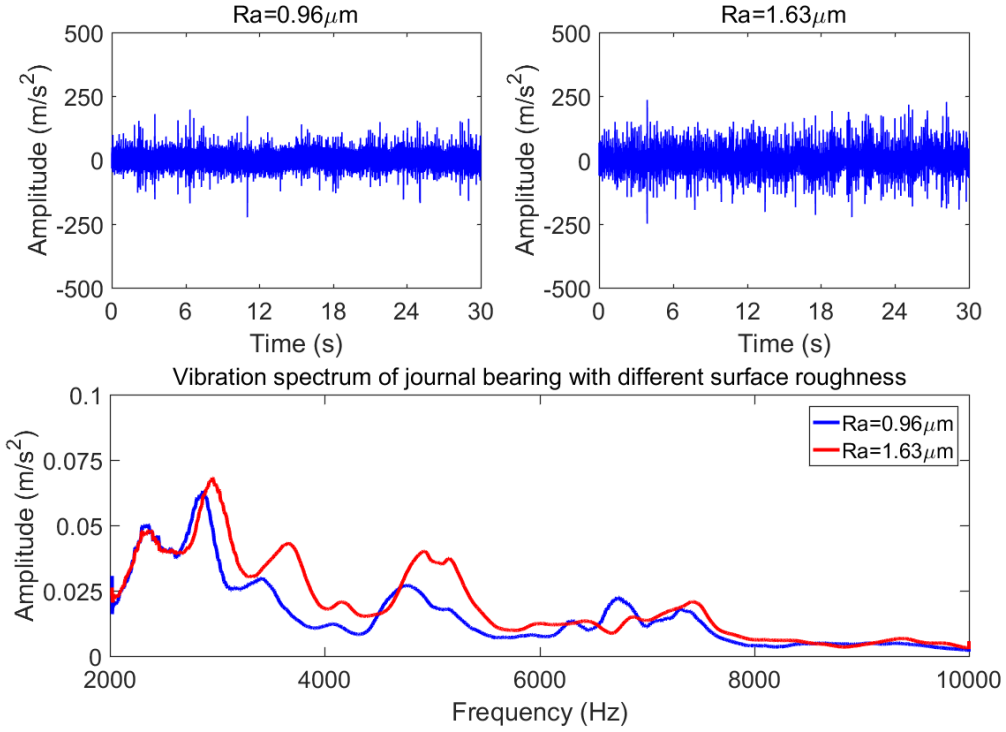

Figure 15. Random vibration of the bearing with different surface roughness

Let these two shafts operate under the same working conditions: the rotational speed of 1650rpm, the lubricant viscosity of 0.015Pas, without any external radial load. The spectra of the acceleration signals acquried from the housing are shown in Fig. 15. The comparison of the vibration amplitude implies that random vibration is directly related to the surface roughness of the rotating journal. Large Ra and more components in low spatial frequency range could lead to the strong intensity of the random excitation.

4.4. Effects of operating condition on random vibration

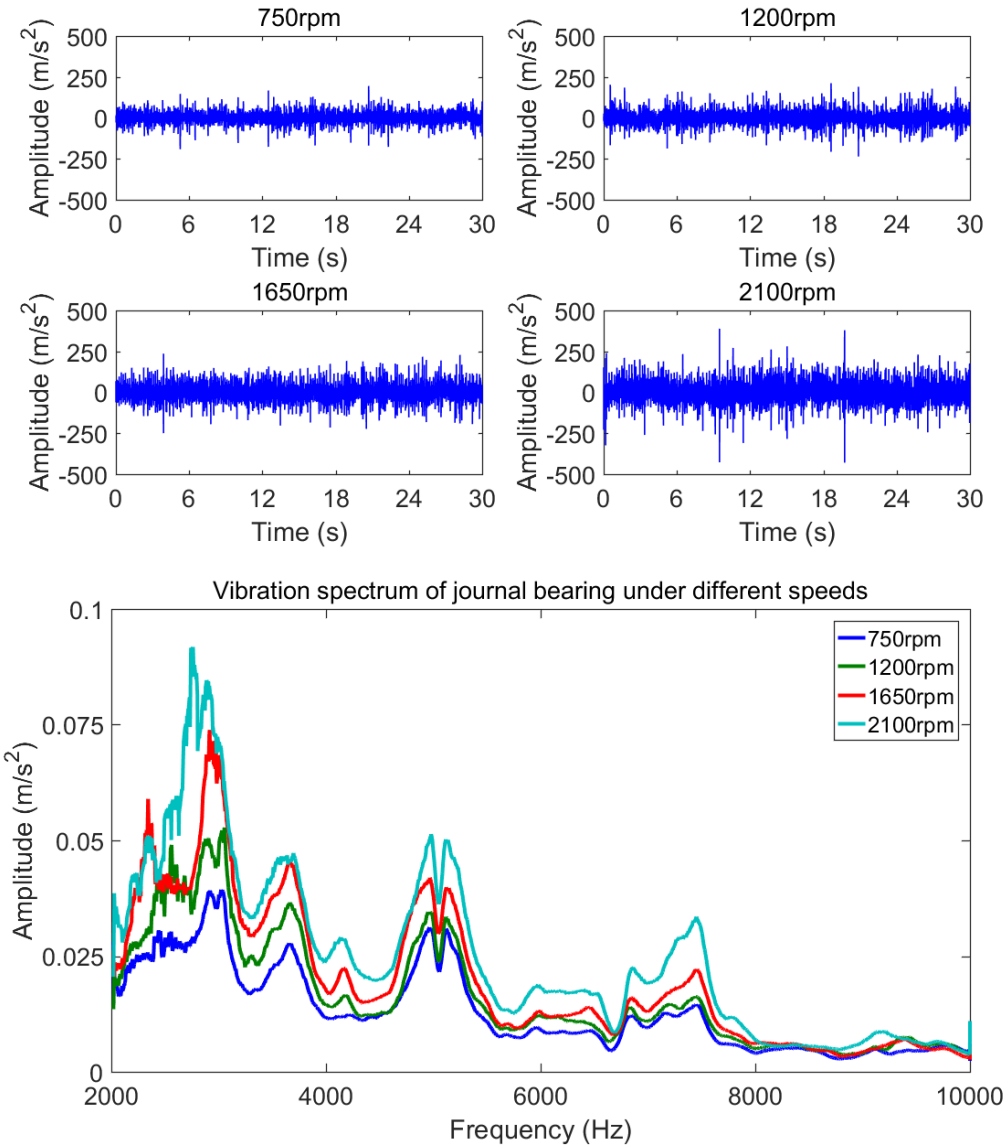

Figure 16. Random vibration of the bearing under different rotational speeds

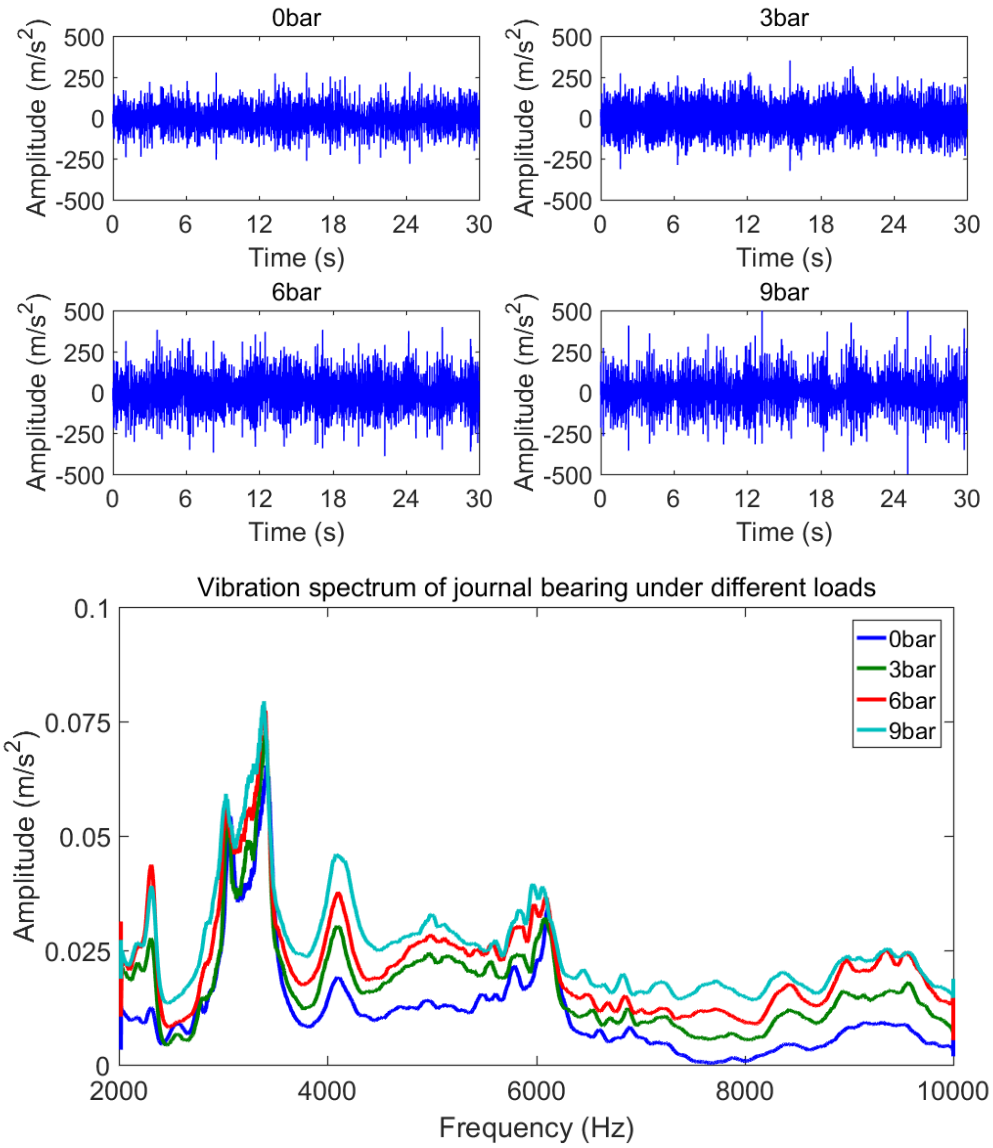

Figure 17. Random vibration of the bearing under different external radial loads

Fig. 16 shows random vibration of the bearing under different rotational speeds without external radial loads. As the rotational speed increases from 750rpm to 2100rpm, vibration amplitudes increase within the whole frequency range. The similar trend can be observed between the vibration amplitude and radial load under the same rotational speed of 1650rpm, which is shown in Fig. 17. The experimental data agree well with the simulation results.

4.5. Fault diagnosis of abrasive wear

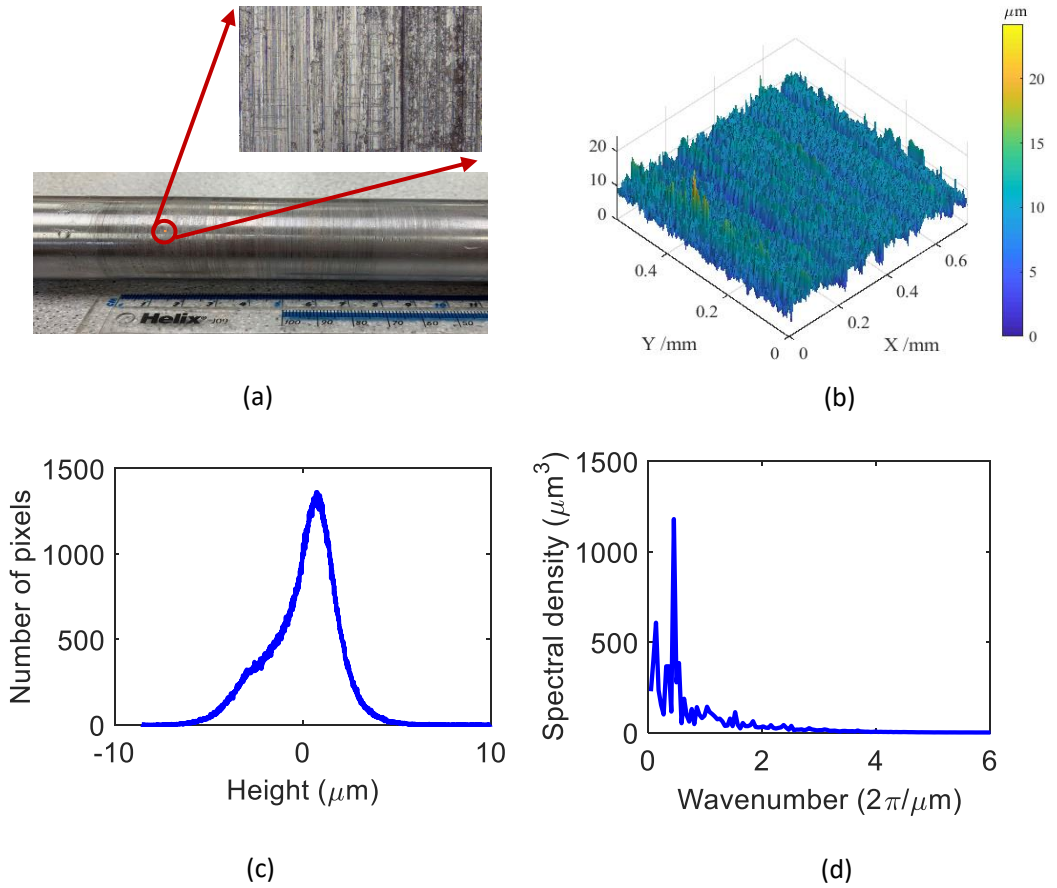

Figure 18. Surface topography of the worn journal on shaft 3:
(a) photomicrograph (b) 3D profile (c) asperities' height distribution (d) spectral density

Fig. 18 shows the surface topography of journal on shaft 3 on which abrasive wear marks are visible. Ra of the journal on shaft 3 is 2.51μm. A number of deep valleys appear on the surface. The asperities' height distribution shown in Fig. 18(c) implies that the average peak-to-peak values increase compared to the healthy journal surfaces. Narrowband spatial components with large amplitudes appear and distribute at low frequency range. With the journal spins, these components may form strong random excitations a narrowband frequency range that is related to the rotational speed.

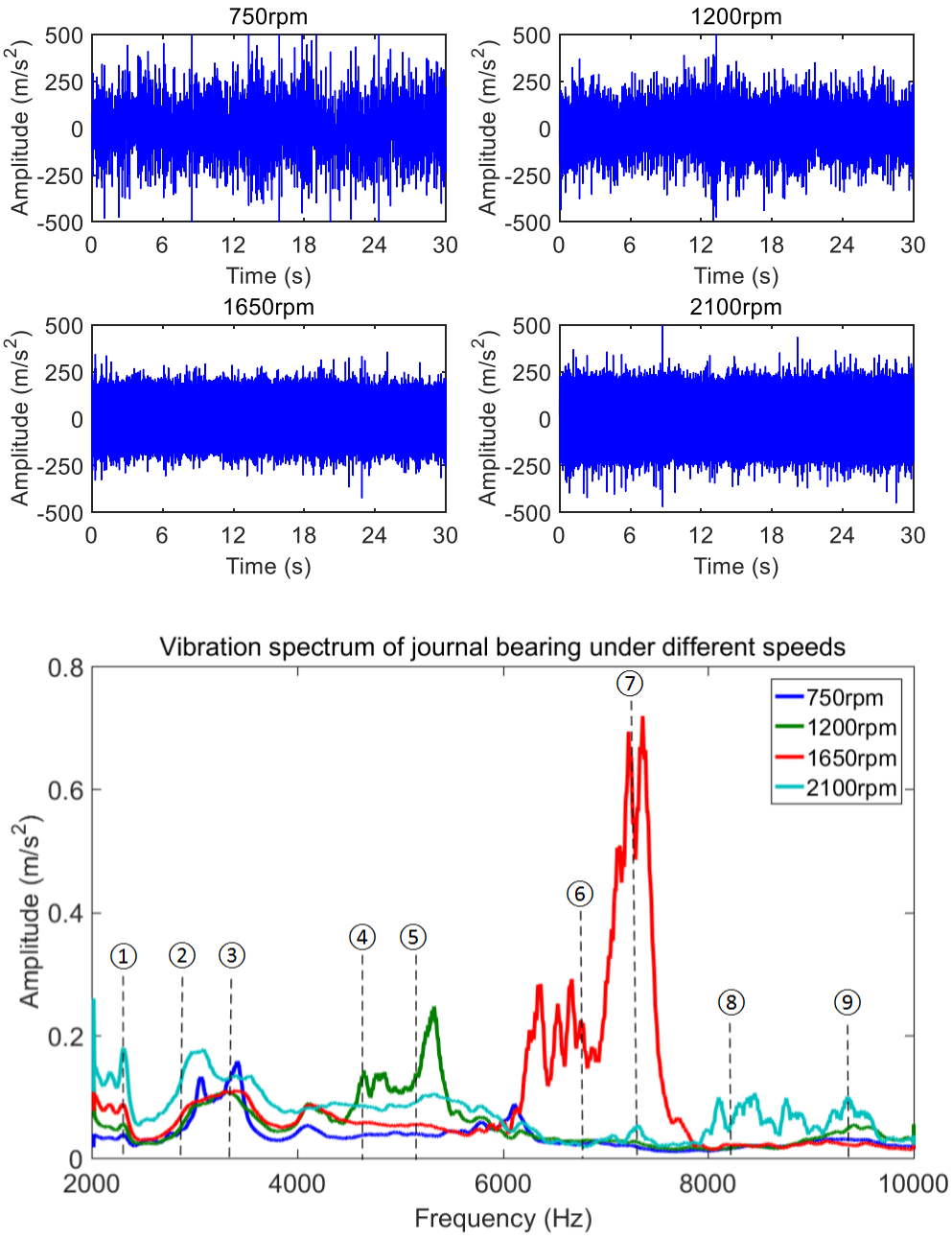

Figure 19. Random vibration of the bearing with a worn journal under different rotational speeds

Let the worn journal operate under different rotational speeds without exerting any external radial loads. Random vibration signals are acquired from the bearing and shown in Fig. 19. Compared to the waveforms in time domain, vibration spectrum clearly exhibits the fault characteristics of abrasive wear. At the speed of 750rpm, vibration components within the frequency range of 2700Hz and 3600Hz appears obviously higher than others, even similar to the corresponding components at the speeds of 1200rpm and 1650rpm. It should be due to the excitation from such narrowband spatial components of the worn journal. Resonant vibrations of the bearing of modes 2 and 3 covered by such frequency band are excited. Increasing the rotational speed to 1200rpm, vibration components with high amplitude appear within the frequency range of 4400Hz and 5700Hz. Resonant vibrations of the bearing of modes 4 and 5 are excited. Further increasing the speed to 1650rpm, the amplitude of vibration components within the frequency range of 5900Hz

and 7800Hz is dramatically increased corresponding to the resonant vibration of the bearing of modes 6 and 7. At the speed of 2100rpm, the vibration components with high amplitude appear within the frequency range of 7900Hz and 9800Hz, and resonant vibrations of the bearing of modes 8 and 9 are excited by the narrowband spatial components of the worn journal. It is illustrated from the vibration spectrum under different rotational speeds that the narrowband spatial components of journal introduced by abrasive wear could form a relatively strong narrowband excitation on the bearing. The covered modes of the bearing could be excited with high amplitudes. Moreover, as the rotational speed increases, the bandwidth becomes linearly wider and more modes of the bearing might be excited. It should be noted that the amplitudes do not vary linearly with the rotational speed due to different damping ratio for different modes.

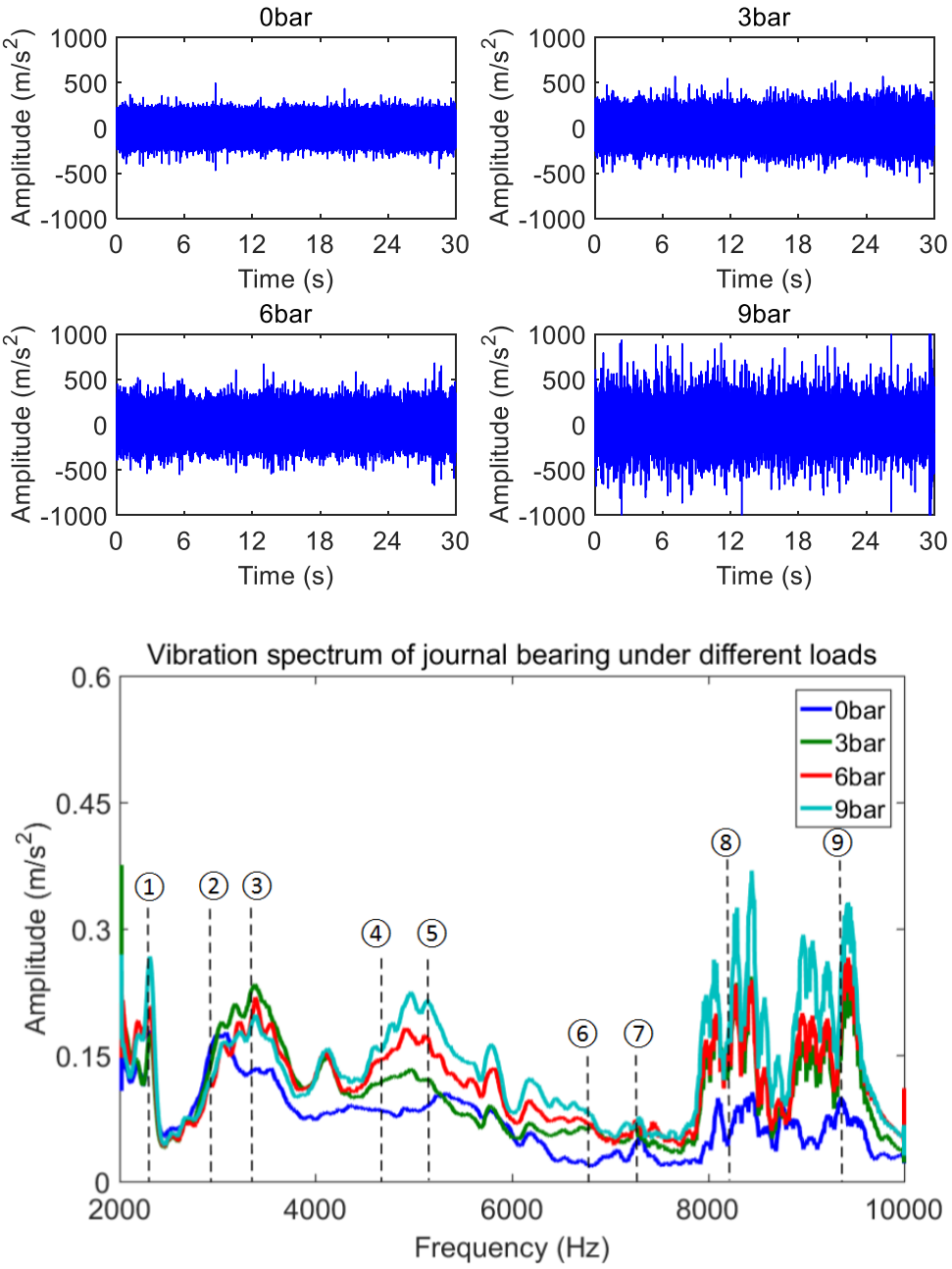

Figure 20. Random vibration of the bearing with a worn journal under different radial loads

Random vibration of the bearing with a worn journal under different radial loads is shown in Fig.

20. The rotational speed is set as 2100rpm. As the radial loads increase, the vibration amplitudes increase within the whole frequency band of interest. The trend is similar to that with heathy journals. A conclusion could therefore be drawn that such speed dependent vibrational behaviours could be viewed as an indicator of the abrasive wear occurrence.

5. Conclusions

This paper presents an investigation on the FAI induced random vibration of hydrodynamic journal bearings aiming to pave a theoretical foundation for condition monitoring of journal bearings and fault diagnosis of abrasive wear in an early stage. A tribo-dynamic model is developed for the FAI in journal bearings. The MPF, which is treated to be the response of rotating journal as displacement excitation through fluid film as a transfer path, induced random excitation is derived. The effects of surface roughness and operating condition on the random excitation are numerically and experimentally investigated. The comparison between random vibration of the journal bearing with healthy and worn journal surface is also evaluated. The main findings are concluded as follows:

The time-varying fluid film thickness due to rotating rough journal surface could give rise to the phenomenon of MPF acted on journal and bearing simultaneously. The MPF exists within a rather wide frequency range, but unlike white noise, most of the power distributes within a certain frequency range, which depends on the spatial spectral density of journal surface and the rotational speed. Surface components at low spatial frequencies could form stronger fluctuation than those with high spatial frequencies. Resonant vibration of the bearing covered within such bandwidth could be excited.

The excitation intensity of MPF is mainly related to the surface roughness of journal and the operating condition. The journal's surface roughness mainly affects either amplitude or power distribution of the displacement excitation, while the operating condition mainly affects the equivalent FRF of fluid film. As the standard deviation of journal surface increases, the displacement excitation rises and the intensity of MPF thereby enlarges. As the correlation length of journal rises, more power distributes within the relatively low frequency range, and thus the intensity of MPF slightly increases. As rotational speed or eccentricity ratio increases, the amplitude amplification ratio of fluid film becomes larger, and thus the stronger intensity of MPF is excited.

The narrowband spatial components of journal introduced by abrasive wear could form a relatively strong narrowband excitation acted on the journal bearing. The covered modes of the bearing could be excited with high amplitudes. As the rotational speed increases, the bandwidth becomes linearly wider and more modes of the bearing might be excited. Such speed dependent vibrational behaviours could be viewed as an indicator of the abrasive wear occurrence.

Acknowledgements

This work was supported by the National Natural Science Foundation of China (Grant no. 51705127), Natural Science Foundation of Hebei Province (Grant no. E2020202017).

References

[1] Y.S. Wang, Q.H. Ma, Q. Zhu, X.T. Liu, L.H. Zhao, An intelligent approach for engine fault diagnosis based on Hilbert-Huang transform and support vector machine, Appl. Acoust. 75 (2014) 1-9.

[2] J. Sun, L. Wang, J. Li, F. Li, J. Li, H. Lu, Online oil debris monitoring of rotating machinery: A detailed review of more than three decades, Mech. Syst. Signal. Pr. 149 (2021) 107341.

[3] K.F. Dufrane, J.W. Kannel, T.H. Mccloskey, Wear of steam turbine journal bearings at low operating speeds, Trans. ASME. J. Lubr. Technol. 105 (1983) 313-317.

[4] H. Hashimoto, S. Wada, K. Nojima, Performance characteristics of worn journal bearings in both laminar and turbulent regime. Part 1: steady-state characteristics, ASLE. Trans. 29 (1986) 565-571.

[5] M. Fillon, J. Bouyer, Thermohydrodynamic analysis of a worn plain journal bearing, Tribol. Int. 37 (2004) 129-136.

[6] S. Akbarzadeh, M.M. Khonsari, Thermoelastohydrodynamic analysis of spur gears with consideration of surface roughness, Tribol. Lett. 32 (2008) 129-141.

[7] A. Beheshti, M.M. Khonsari, A thermodynamic approach for prediction of wear coefficient under unlubricated sliding condition, Tribol. Lett. 38 (2010) 347-354.

[8] D.E. Sander, H. Allmaier, H.H. Priebsch, Simulation of journal bearing friction in severe mixed lubrication-validation and effect of surface smoothing due to running-in, Tribol. Int. 96 (2015) 173-183.

[9] D.E. Sander, A. Hannes, Starting and stopping behaviour of worn journal bearings, Tribol. Int. 127 (2018) 478-488.

[10] G. Xiang, Y.F. Han, J.X. Wang, J.F. Wang, X.K. Ni, Coupling transient mixed lubrication and wear for journal bearing modeling, Tribol. Int. 138 (2019) 1-15.

[11] F. König, A.O. Chaib, G. Jacbos, C. Sous, A multiscale-approach for wear prediction in journal bearing systems – from wearing-in towards steady-state wear, Wear, 426-427 (2019) 1203-1211.

[12] D. Gropper, L. Wang, T.J. Harvey, Hydrodynamic lubrication of textured surfaces: A review of modelling techniques and key findings, Tribol. Int. 94 (2016) 509-529.

[13] M.B. Dobrica, M. Fillon, P. Maspeyrot, Mixed elastohydrodynamic lubrication in a partial journal bearing – comparison between deterministic and stochastic models, J. Tribol. 128 (2006) 778-788.

[14] C.W. Chan, Y.F. Han, Z.J. Wang, J.X. Wang, F.H. Shi, N.Z. Wang, Q.J. Wang, Exploration on a fast EHL computing technology for analysing journal bearings with engineered surface textures, Tribol. Trans. 57 (2013) 206-215.

[15] F. Sahlin, R. Larsson, A. Almqvist, P.M. Lugt, P. Marklund, A mixed lubrication model incorporating measured surface topography. Part 1: theory of flow factors, Proc. Inst. Mech. Eng. Part J: J. Eng. Tribol. 224 (2010) 335-351.

[16] F. Sahlin, R. Larsson, P. Marklund, A. Almqvist, P.M. Lugt, A mixed lubrication model incorporating measured surface topography. Part 2: roughness treatment, model validation, and simulation. Proc. Inst. Mech. Eng. Part J: J. Eng. Tribol. 224 (2010) 353-365.

[17] H.M. Checo, D. Dureisseix, N. Fillot, J. Raisin, A homogenized micro-elastohydrodynamic lubrication model: Accounting for non-negligible microscopic quantities, Tribol. Int. 135 (2019) 344-354.

[18] Q.J. Wang, D. Zhu, R. Zhou, F. Hashimoto, Investigating the effect of surface finish on mixed EHL in rolling and rolling-sliding contacts, Tribol. Trans. 51 (2008) 748-761.

[19] C.X. Gu, X.H. Meng, Y.B. Xie, J.Z. Fan, A thermal mixed lubrication model to study the textured ring/liner conjunction, Tribol. Int. 101 (2016) 178-193.

[20] C.C. Fang, X.H. Meng, Y.B. Xie, A piston tribodynamic model with deterministic consideration of skirt surface grooves, Tribol. Int. 110 (2017) 232-251.

[21] X.K. Wang, Q. Xu, B.R. Wang, L.X. Zhang, H. Yang, Z.K. Peng, Effect of surface waviness on the static performance of aerostatic journal bearings, Tribol. Int. 103 (2016) 394-405.

[22] A.F. Quiñonez, G.E. Morales-Espejel, Surface roughness effects in hydrodynamic bearings, Tribol. Int. 98 (2016) 212-219.

[23] N. Patir, H. S. Cheng, An average flow model for determining effects of three-dimensional roughness on partial hydrodynamic lubrication, J. Lubr. Technol. 100 (1978) 12-17.

[24] Y. Hu, K. Tonder, Simulation of 3-D random rough surface by 2-D digital filter and fourier analysis, Int. J. Mach. Tools Manu. 32 (1992) 83-90.

[25] P.V. Overschee, B.D. Moor, Subspace identification for linear systems: Theory-Implementation-Applications, Kluwer Academic Publishers, The Netherlands, 2011.